Chemical Science

ROYAL SOCIETY OF CHEMISTRY

EDGE ARTICLE

View Article Online
View Journal | View Issue

Check for updates

Cite this: *Chem. Sci.*, 2021, **12**, 11740

All publication charges for this article have been paid for by the Royal Society of Chemistry

A highly sensitive and selective fluoride sensor based on a riboswitch-regulated transcription coupled with CRISPR-Cas13a tandem reaction†

Yuan Ma, [ab] Quanbing Mou,[a] Peng Yan, [ac] Zhenglin Yang,[d] Ying Xiong,[a] Deyue Yan, [b] Chuan Zhang, *[b] Xinyuan Zhu *[b] and Yi Lu *[ad]

Nucleic acid sensors have realized much success in detecting positively charged and neutral molecules, but have rarely been applied for measuring negatively charged molecules, such as fluoride, even though an effective sensor is needed to promote dental health while preventing osteofluorosis and other diseases. To address this issue, we herein report a quantitative fluoride sensor with a portable fluorometer readout based on fluoride riboswitch-regulated transcription coupled with CRISPR-Cas13-based signal amplification. This tandem sensor utilizes the fluoride riboswitch to regulate *in vitro* transcription and generate full-length transcribed RNA that can be recognized by CRISPR-Cas13a, triggering the collateral cleavage of the fluorophore-quencher labeled RNA probe and generating a fluorescence signal output. This tandem sensor can quantitatively detect fluoride at ambient temperature in aqueous solution with high sensitivity (limit of detection (LOD) ≈ 1.7 μM), high selectivity against other common anions, a wide dynamic range (0–800 μM) and a short sample-to-answer time (30 min). This work expands the application of nucleic acid sensors to negatively charged targets and demonstrates their potential for the on-site and real-time detection of fluoride in environmental monitoring and point-of-care diagnostics.

Received 28th June 2021
Accepted 20th July 2021

DOI: 10.1039/d1sc03508h

rsc.li/chemical-science

Open Access Article. Published on 09 August 2021. Downloaded on 2/11/2026 8:37:09 PM.
This article is licensed under a Creative Commons Attribution-NonCommercial 3.0 Unported Licence.

Introduction

Functional nucleic acids,[1,2] such as aptamers,[3–7] riboswitches,[8,9] ribozymes,[10–13] and DNAzymes,[14–18] have emerged as a major class of sensors for on-site and real-time detections in applications such as environmental monitoring[19,20] and point-of-care diagnostics[21–24] of a wide range of targets with high selectivity.[25–30] Despite the progress, these functional nucleic acid sensors work well mainly for positively charged or neutral molecules. Although anions are important analytes,[31] only one nucleic acid sensor has been reported for chloride imaging, which utilizes a nucleic acid strand conjugated with an anion-specific organic molecule for sensing.[32] Among these anions, fluoride is one of the most attractive targets due to its significant association with biological, medical, industrial, and environmental processes.[33–35] On one hand, as an essential element for living organisms, fluoride plays an important role in dental health[36] and has the potential for the treatment of osteoporosis.[37] On the other hand, fluoride is easily accumulated in organisms with slow excretion,[38] which may cause excess fluoride ingestion to induce pathological conditions, including fluorosis,[39] urolithiasis, osteoporosis, neurological and metabolic dysfunction, gastric and kidney problems, and certain types of cancer.[34,40,41] Since fluoride is widely used, the fluoride contamination in the environment and drinking water may raise major concerns. Therefore, the United States Environmental Protection Agency (EPA) sets an enforceable drinking water standard for fluoride of 4 mg mL^{-1} (211 μM) to prevent osteofluorosis and other diseases, and a secondary non-enforceable fluoride standard of 2 mg mL^{-1} (105 μM) to promote dental health.[42] As a result, the optimal range of fluoride concentration between deficiency (2 mg mL^{-1}) and toxicity (4 mg mL^{-1}) is quite narrow. Therefore, the accurate determination of fluoride concentration in drinking water that can cover this narrow concentration range is required.

To meet the above goal, several analytical methods have been developed for fluoride detection, including ^{19}F NMR analysis, mass spectrometry, and atomic absorption spectrophotometry, standard Willard and Winter methods, fluoride selective electrodes, and ion chromatography.[43,44] However, these instrumental analyses require expensive equipment, complicated procedures, and skilled operators, making these methods not

[a]*Department of Chemistry, University of Illinois at Urbana-Champaign, Urbana, Illinois 61801, USA. E-mail: yi-lu@illinois.edu*

[b]*School of Chemistry and Chemical Engineering, Frontiers Science Center for Transformative Molecules, Shanghai Jiao Tong University, 800 Dongchuan Road, Shanghai 200240, China. E-mail: xyzhu@sjtu.edu.cn; chuanzhang@sjtu.edu.cn*

[c]*Key Laboratory of Biomedical Information Engineering of Ministry of Education, School of Life Science and Technology, Xi'an Jiaotong University, 710049, Xi'an, PR China*

[d]*Department of Biochemistry, University of Illinois at Urbana-Champaign, Urbana, Illinois 61801, USA*

† Electronic supplementary information (ESI) available. See DOI: 10.1039/d1sc03508h

© 2021 The Author(s). Published by the Royal Society of Chemistry

Open Access Article. Published on 09 August 2021. Downloaded on 2/11/2026 8:37:09 PM. This article is licensed under a Creative Commons Attribution-NonCommercial 3.0 Unported Licence.

affordable for on-site or point-of-care (POC) application.[43] Besides, fluoride selective electrodes are easily affected by temperature, interfering ions, color of the sample, shift potential, and ion activity, and require skilled operators to ensure accuracy.[43] In addition, other analytical methods are not portable, which greatly limits their applications for on-site and real-time detection.[34] To address this issue, optical chemosensors have attracted great attention for developing POC fluoride sensors, due to their simple procedure and high sensitivity and selectivity, along with real-time detection.[34,45] Therefore, many different optical fluoride sensors with fluorescent and colorimetric readouts have been developed based on various mechanisms, such as interactions between fluoride ions and Lewis acids,[33,46] fluoride–hydrogen bond interactions,[33,47] reaction based chemodosimeters,[35,42,48] and interaction with other types of materials.[49–51] Despite the progress made, portable fluoride detection is still not available to the general public, because very few sensors can meet all these requirements: (1) good performance in aqueous solution; (2) high selectivity for fluoride without interference from other anions; (3) detection range covering the deficiency and toxicity lines in the EPA standards; and (4) short response time.

To address this issue, we take advantage of the fluoride-binding riboswitch that has recently been discovered in bacteria and archaea.[52–54] The high selectivity of the fluoride riboswitch toward fluoride over other halides or anions has been attributed to the smaller ionic radius of fluoride (0.133 nm) than other chemical species, including chloride (0.181 nm), as well as the unique hydrogen bonding abilities of fluoride.[52,53] A crystal structure of the riboswitch has shown that the riboswitch folds into a 3D structure, and coordinates with three Mg^{2+} ions, which allows binding one F^-, but not enough space to bind other anions.[52,53] In the absence of fluoride, the ligand-free fluoride riboswitch transiently accesses a low-populated (~1%) and short-lived (~3 ms) excited conformational state, which unravels a conserved 'linchpin' base pair to signal transcription termination.[55] In the presence of fluoride, this highly localized, fleeting process is allosterically suppressed, which activates transcription.[55] Therefore, the fluoride riboswitch can activate transcription in the presence of fluoride, which can regulate gene expression encoding fluoride transporters to remove fluoride as a native defense mechanism against fluoride toxicity.[55,56] Moreover, the fluoride riboswitch can regulate *in vitro* transcription to generate full-length transcribed RNA depending on the fluoride concentration,[55] where a higher concentration of fluoride results in a larger number of full-length RNA transcripts. To convert such a highly selective fluoride-regulated transcription into a signal that can be readily detected by a portable fluorometer, we employ CRISPR-Cas13 (Clustered Regularly Interspaced Short Palindromic Repeats-associated system), which can recognize a target RNA through a sequence complementary to CRISPR RNA (crRNA), and then collaterally cleave a nearby reporter fluorophore/quencher pair with an RNA spacer, resulting in the fluorophore moving away from the quencher and thus an increase of the fluorescent signal.[57–62] Due to this unique property, the CRISPR-Cas13-based sensors have been applied to detect diverse targets, such as nucleic acids,[63–69] epigenetic base modification,[70] viruses,[71–74] bacteria,[75,76] and small molecules.[77] For instance, a CRISPR-Cas13-based sensor called SPRINT was able to detect 8 small molecules including fluoride.[77] Despite the progress, the current nucleic acid based fluoride detection system has a narrow detection dynamic range of 1 to 100 μM, with a drastically decreased signal at fluoride concentrations above 100 μM. Since the EPA standard for fluoride is 211 μM (4 mg L^{-1}), the detection range of the SPRINT system is above the threshold level defined by the EPA and therefore cannot be used as an on-site sensor for detecting fluoride in drinking water and differentiating whether the water is safe or not.

To address the current limitations of fluoride sensors, we report herein a Fluoride RiboswItch-regulated Transcription with Cas13a (FRITCas13a) tandem sensor, by coupling the fluoride riboswitch-regulated transcription with CRISPR-Cas13a-based cleavage of reporter RNA activated by the transcribed RNA. The system can quantitatively detect fluoride at ambient temperature in aqueous solution with a wide dynamic range (0–800 μM), a low limit of detection (LOD ≈ 1.7 μM), and a short sample-to-answer time (30 min) using a portable fluorometer, demonstrating high potential for on-site and real-time detection and quantification of fluoride in drinking water and other types of samples.

Results and discussion

The FRITCas13a tandem sensor involves fluoride-riboswitch regulated *in vitro* transcription along with Cas13a-mediated collateral cleavage of the reporter RNA (Scheme 1). Specifically, the binding of fluoride by its riboswitch will activate *in vitro* transcription and generate full-length RNA transcripts, which carry a Cas13a targeting RNA sequence at the 3′-end from the *in vitro* transcription. The transcribed Cas13a targeting RNA then hybridizes with crRNA to activate the Cas13a-mediated collateral cleavage of a reporter RNA with a fluorophore (FAM) at the 5′-end and a quencher (BHQ1) at the 3′-end. Without the Cas13a-mediated collateral cleavage, the reporter RNA has a low fluorescent signal because the quencher is close to the fluorophore and thus quenched the fluorescence. In the presence of fluoride, the full-length RNA transcripts activate Cas13a to cleave the reporter RNA and release the quencher from the fluorophore and thus recover a significant fluorescence signal. In this design, the fluoride concentration in the sample is positively correlated with the copies of full-length RNA transcripts, the reporter RNA cleavage, and the fluorescence signal generation. Moreover, this FRITCas13a tandem sensor can both detect and quantify fluoride in aqueous solution. In contrast, in the absence of fluoride, the regulation effect of the fluoride riboswitch will result in partially transcribed RNA lacking the Cas13a targeting sequence at the 3′-end.[55] As a result, the collateral cleavage of the reporter RNA by Cas13a will not occur and a minimal fluorescence signal will be observed.

To demonstrate such a FRITCas13a tandem sensor, we take advantage of the *in vitro* transcription system reported by Zhang's group with a wide and tunable dynamic range between 0.01 and 100 mM.[55] The DNA templates were prepared by

Open Access Article. Published on 09 August 2021. Downloaded on 2/11/2026 8:37:09 PM.
This article is licensed under a Creative Commons Attribution-NonCommercial 3.0 Unported Licence.

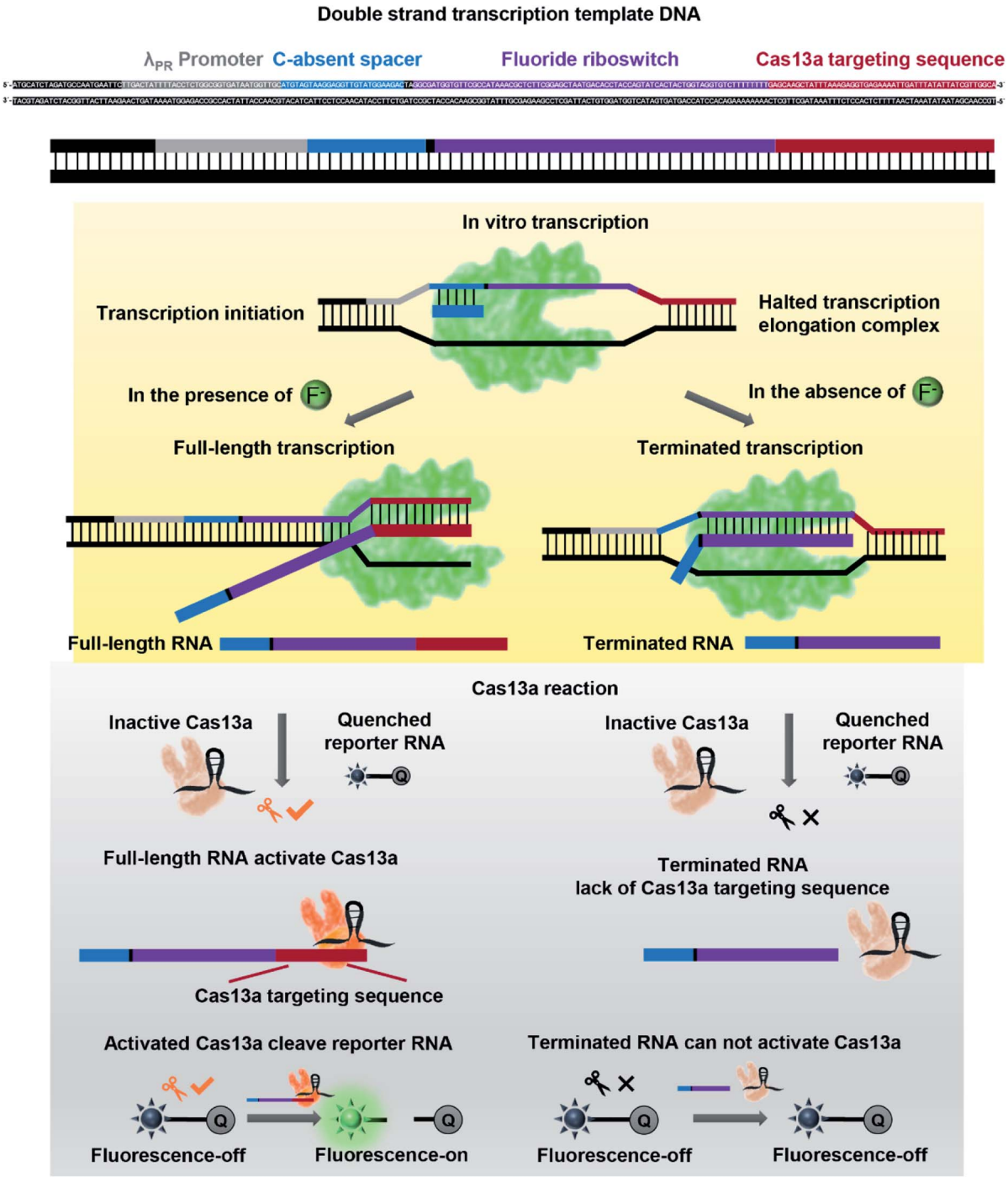

Scheme 1 Detection strategy and workflow of a fluoride riboswitch-regulated transcription with a Cas13a (FRITCas13a) tandem sensor for detecting fluoride in aqueous solution.

ligation from shorter DNA units consisting of a λ_{PR} promoter, C-absent spacer, fluoride riboswitch and Cas13a targeting sequence at the 3′-end (Scheme 1, Fig. S1, Table S1†). The formation of the DNA templates was verified by 10% denaturing polyacrylamide gel electrophoresis (PAGE) gel analysis (see Fig. S2†). Moreover, the obtained DNA templates were then purified and extracted from the PAGE gel and used for *in vitro* transcription. To verify that the transcription is regulated by fluoride in a wide range of concentrations, fluoride-dependent transcription with different concentrations of NTP was performed. As shown in Fig. 1, S3 and S4,† the transcription readthrough, defined by full-length RNA/(full-length RNA + terminated RNA), is regulated by the fluoride concentration from 0–1 mM at different NTP concentrations of 10, 20, and 30 μM. Moreover, to develop a fluoride sensor with high sensitivity, the transcription reaction was optimized with various reaction

© 2021 The Author(s). Published by the Royal Society of Chemistry

Open Access Article. Published on 09 August 2021. Downloaded on 2/11/2026 8:37:09 PM.
This article is licensed under a Creative Commons Attribution-NonCommercial 3.0 Unported Licence.

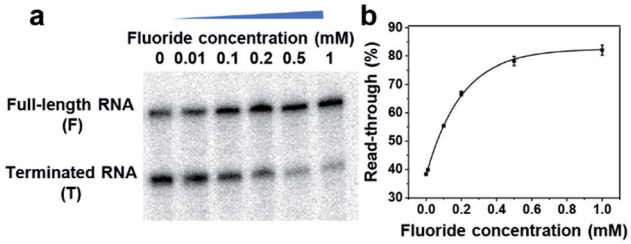

Fig. 1 Fluoride-dependent single-round transcription assay with 30 μM NTP. (a) Autoradiogram of a 10% PAGE denaturing gel separating the full-length (*F*) and terminated (*T*) RNA products; (b) fluoride-dependent transcription readthrough, calculated by using $F/(F + T)$.

temperatures of 25, 30, and 37 °C to increase the signal-to-noise ratio. As shown in Fig. S5 and S6,† the transcription reaction at 37 °C generated a higher readthrough ratio than those at 25 and 30 °C. Thereafter, 37 °C was chosen as the optimal transcription reaction temperature.

Having demonstrated that the fluoride riboswitch-regulated transcription can transform its binding of the fluoride into full-length transcribed RNA quantitively, we applied Cas13a to detect the transcribed RNA and then generate a fluorescence readout to act as a tandem sensor for fluoride detection. To achieve good analytical performance of the fluoride sensor, several parameters of the Cas13a reaction were optimized, including reaction buffer, reaction time and quenching method. First, we evaluated three commercialized or literature reported buffers,[57,65] and found that buffer 1 (ref. 57) showed the best performance, due to its highest Cas13a cleavage activity and signal to noise ratio (Fig. S7†). Moreover, the kinetics of the tandem reaction were investigated by monitoring real-time fluorescence using a plate reader, which include the transcription of the full-length RNA and then the cleavage of the reporter RNA by Cas13a. As shown in Fig. 2a, 15 and 30 min were chosen as good time frames to perform detection, which not only ensure sufficient signal intensity but also reduce the sample-to-answer time. To control the reaction time more precisely, the quenching method for the tandem reaction was further studied by quenching the reaction at 65 °C or 85 °C for 10 min and then tracking real-time fluorescence using a plate reader. As shown in Fig. S8,† a steady fluorescence signal after reaction ends was obtained after quenching the reaction at 65 °C or 85 °C for 10 min. Considering that lower temperature will be beneficial for the stability of reporter RNA, the reaction quenching at 65 °C for 10 min was chosen for the subsequent experiments.

To apply the FRITCas13a tandem sensor for fluoride detection, the above optimized tandem reaction workflow was performed for 30 min with the addition of different concentrations of fluoride and then measurement of fluorescence spectra of the sensors by using a fluorometer. As shown in Fig. 2b, the fluorescence intensity increases corresponding to the elevation of fluoride concentrations. By plotting the relative fluorescence ratio ($(F - F_0)/F_0$) against the fluoride concentration, where F and F_0 are derived in the presence and absence of fluoride respectively, we obtained a binding curve and the LOD was calculated to be 1.7 μM (Fig. 2c), based on $3\sigma_b$/slope, where σ_b is

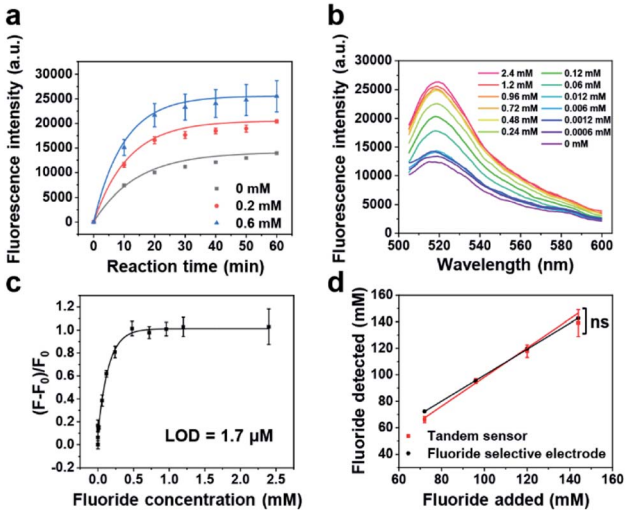

Fig. 2 Quantitative detection of fluoride by the FRITCas13a tandem sensor. (a) Reaction kinetics of the tandem sensor monitored by a plate reader in the presence of 0, 0.2, and 0.6 mM fluoride; (b) fluorescence spectra of the tandem reaction sensor at different fluoride concentrations with a 30 min detection time; (c) the $(F - F_0)/F_0$ of the tandem sensor at different fluoride concentrations with a 30 min detection time; (d) comparison of the tandem sensor with an EPA approved method, a fluoride selective electrode using fluoride spiked samples. Statistical significance: ns: no significant difference; $^*P < 0.05$; $^{**}P < 0.01$; $^{***}P < 0.001$.

the standard deviation of three blank samples. The LOD of this sensor is ~16 fold lower than that of the EPA standard method using a fluoride selective electrode (26.3 μM).[78] Moreover, to further shorten the detection time, the same test was performed for 15 min with the addition of different concentrations of fluoride. As shown in Fig. S9,† the relative fluorescence ratios ($(F - F_0)/F_0$) increase corresponding to the elevation of fluoride concentrations. Based on the $3\sigma_b$/slope method, within a detection time of 15 min, the LOD of sensor was calculated to be 2.5 μM.

The selectivity of our sensor was also examined by performing the test in the presence of fluoride or many potentially interfering analytes at a concentration of 200 μM. As shown in Fig. 3, the sensor displays a weak or negligible response to most anions, including heavier halides (Cl^-, Br^-, and I^-), other inorganic anions (CO_3^{2-}, HCO_3^-, SO_4^{2-}, $H_2PO_4^-$, HPO_4^{2-}, and NO_3^-), and organic anions ($HCOO^-$ and CH_3COO^-), while the fluorescence signal in the presence of fluoride is significantly higher than that of the other anions ($p < 0.001$). Moreover, considering that real environmental samples may contain anion mixtures instead of individual ones, we tested the fluoride sensor in the presence of various anion mixtures, such as a mixture of four different common anions in the environment (Cl^-, NO_3^-, CO_3^{2-}, and SO_4^{2-}, 50 μM for each anion), and 11 different anion mixtures (Cl^-, Br^-, I^-, CO_3^{2-}, HCO_3^-, SO_4^{2-}, $H_2PO_4^-$, HPO_4^{2-}, NO_3^-, $HCOO^-$, and CH_3COO^-, 18 μM for each anion). As shown in Fig. S10,† the sensor displays a weak or negligible response to anion mixtures compared with the signal in the presence of fluoride ($p < 0001$), demonstrating that

Open Access Article. Published on 09 August 2021. Downloaded on 2/11/2026 8:37:09 PM.
This article is licensed under a Creative Commons Attribution-NonCommercial 3.0 Unported Licence.

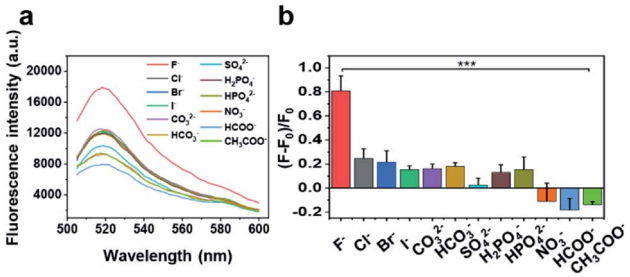

Fig. 3 The selectivity of the FRITCas13a tandem sensor against common anions, including Cl^-, Br^-, I^-, CO_3^{2-}, HCO_3^-, SO_4^{2-}, $H_2PO_4^-$, HPO_4^{2-}, NO_3^-, $HCOO^-$, and CH_3COO^-. The fluorescence spectra (a) and the $(F - F_0)/F_0$ value (b) of the FRITCas13a tandem sensor in the presence of F^- and diverse anions (200 μM).

the sensor maintains high selectivity toward fluoride even in the presence of anion mixtures.

The detection of fluoride with the fluoride sensor in real samples may potentially be affected by common interferents, such as cations, anions, DNAse, RNAse, or protease. Thus, tests in the presence of those common interferents were conducted. To investigate the interference of common cations, such as Na^+, K^+, Mg^{2+}, and Ca^{2+}, we performed the test at a fluoride concentration of 200 μM in the absence or presence of each cation (100 μM). The selectivity coefficient (SC) for each of the potential interfering agents was calculated using the formula, $SC = A_{c+i}/A_c$, where A_{c+i} and A_c are the response for fluoride in the presence and absence of each interfering agent, respectively. As shown in Fig. S11,† the signal was not affected by the presence of Na^+, K^+, Mg^{2+}, and Ca^{2+} as their SC approximates to 1. In addition, to understand the interference by common cation and anion mixtures in real samples, we performed the test in samples spiked with cation mixtures (Na^+, K^+, Mg^{2+}, and Ca^{2+}), or various cation and anion mixtures (Na^+, K^+, Mg^{2+}, Ca^{2+}, Cl^-, NO_3^-, CO_3^{2-}, and SO_4^{2-}). As shown in Fig. S11,† both groups cause minimal interference for the fluoride detection. In addition, the fluoride sensor utilizes *in vitro* transcription and CRISPR-Cas13a mediated amplification, which could be potentially interfered with by DNAses, RNAses, and proteases present in the environmental sample. To address this issue, the environmental samples were heat-pretreated at 95 °C for 10 min to inactivate potential DNAses and proteases, following protocols reported previously.[72,74] Moreover, since RNAses cannot be heat-inactivated, we added an RNAse inhibitor during the tandem reaction. To test the effectiveness of the pretreatment, we spiked the samples with DNAse I, RNAse A, and protease K, heated the samples at 95 °C for 10 min, and then performed the tandem reaction with a RNaseOUT™ Recombinant Ribonuclease Inhibitor, using an unspiked sample as the control. As shown in Fig. S12,† after the pretreatments, DNAse I, RNAse A, and protease K showed minor interference (6%) towards the tandem reaction signal. These results demonstrated that the method we have adopted is effective in minimizing nucleases/proteases from degrading the sensor components.

To examine the accuracy and reliability of our FRITCas13a tandem sensor in real samples, our sensor was compared with an EPA-approved method, a fluoride selective electrode, by analyzing drinking water samples spiked with different concentrations of fluoride using the standard calibration method. As shown in Fig. 2d, the fluoride concentrations detected by the FRITCas13a tandem sensor show a strong positive correlation with the added fluoride concentrations and the concentrations detected by the fluoride selective electrode. Moreover, the slope of fluoride concentration detected by the tandem sensor is 1.01 ± 0.08 ($R^2 = 0.9895$), which is similar to the slope measured by the fluoride selective electrode 0.98 ± 0.01 ($R^2 = 0.9999$). Moreover, the ability of the fluoride sensor to quantify fluoride in real environmental samples was tested with various types of samples, including bottled water from a supermarket, drinking water samples from tap water in Urbana (IL, US), and lake water in Urbana (IL, US). As shown in Fig. S13,† no detectable fluoride was found in the bottled water while fluoride was detected and quantified in both the tap water and the lake water by our fluoride sensor and the results were very similar to those from the standard test using the fluoride selective electrode (Fig. S13†), indicating the accuracy of our sensor. Moreover, unknown samples may contain multiple interferents, which may potentially lead to significant matrix effects and affect the accurate detection. To address this issue, the standard addition method was applied to avoid matrix effects and determine the fluoride concentration by our sensor as in a previous report.[79] As a proof of concept, a tap water sample spiked with fluoride at a final concentration of 450 μM was analyzed using the standard addition method. Briefly, the samples were spiked with fluoride at different additional concentrations for the tandem reaction, and the concentration of real samples can be calculated based on the extrapolation method. As shown in Fig. S14,† according to the calibration curve obtained, the fluoride concentration of the spiked tap water sample was calculated to be 430.5 ± 11.7 μM (recovery yield of 95.7%), which demonstrates similar accuracy to the result obtained by the fluoride selective electrode (463.9 ± 5.3 μM, recovery yield of 103.1%). Therefore, the accuracy and reliability of our sensor are comparable to those of the EPA-approved fluoride selective electrode.

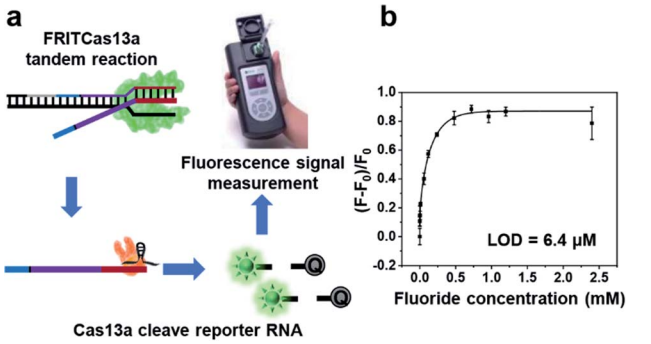

Fig. 4 FRITCas13a tandem sensor based portable device. (a) Workflow for fluoride detection with a portable fluorimeter. (b) Fluorescence signal of the FRITCas13a tandem sensor with different concentrations of fluoride.

© 2021 The Author(s). Published by the Royal Society of Chemistry

Open Access Article. Published on 09 August 2021. Downloaded on 2/11/2026 8:37:09 PM. This article is licensed under a Creative Commons Attribution-NonCommercial 3.0 Unported Licence.

To demonstrate the ability of our fluoride sensor for on-site and real-time detection, we conduct the tandem reaction with the addition of different concentrations of fluoride and then use a commercially available portable fluorimeter as the fluorescence detection device (Fig. 4a). As shown in Fig. 4b, the fluorescence signal increases with the fluoride concentration from 0 to 810 μM, demonstrating a wide dynamic range for fluoride detection. Moreover, the LOD of this POC sensor is calculated to be 6.4 μM, which is 4-fold lower than 26.3 μM obtained when the EPA-certified fluoride selective electrode is used.[78]

Conclusions

In summary, we have developed a fluoride riboswitch-regulated transcription with Cas13a (FRITCas13a) tandem sensor for the quantitative detection of fluoride in aqueous solution. The assay uses a simple and fast workflow, with a sample-to-answer time of 30 min, which includes fluoride-riboswitch regulated transcription and Cas13a-mediated signal amplification and fluorescence output. This system can detect fluoride in aqueous solution quantitatively, with high sensitivity (LOD ≈ 1.7 μM), high selectivity to differentiate fluoride from other common anions, and a wide dynamic range of 0–800 μM. This work has expanded the application of nucleic acid sensors for anion detection, and after integration with a portable fluorometer, allows on-site and real-time detection and quantification of fluoride for both environmental monitoring and POC diagnostics.

Author contributions

Y. M. designed the detection workflow, performed the experiments and wrote the manuscript. Q. M. assisted with project design and fluorescence experiments. P. Y. assisted with the portable fluorometer experiments. Z. Y. and Y. X. participated in designing Cas13a system. D. Y., C. Z., X. Z. mentored the project, revised the manuscript. Y. L. initiated idea, mentored the project, designed the workflow and revised the paper.

Conflicts of interest

The authors declare no conflict of interest.

Acknowledgements

This work was supported by Illinois-JITRI Institute (JITRI 23965) and US National Institute of Health (GM141931). Y. M. acknowledges the National Natural Science Foundation of China (21905170) and China Postdoctoral Science Foundation (2019M651479). We would like to thank Jennifer Cui for her help with the portable fluorimeter experiments.

Notes and references

1 J. Zhang, T. Lan and Y. Lu, *Adv. Healthcare Mater.*, 2019, **8**, e1801158.
2 R. Micura and C. Höbartner, *Chem. Soc. Rev.*, 2020, **49**, 7331–7353.
3 J. Zhang, L. P. Smaga, N. S. R. Satyavolu, J. Chan and Y. Lu, *J. Am. Chem. Soc.*, 2017, **139**, 17225–17228.
4 M. Liu, Q. Yin, Y. Chang, Q. Zhang, J. D. Brennan and Y. Li, *Angew. Chem., Int. Ed. Engl.*, 2019, **58**, 8013–8017.
5 S. Dey and J. T. Sczepanski, *Nucleic Acids Res.*, 2020, **48**, 1669–1680.
6 H. Yu, O. Alkhamis, J. Canoura, Y. Liu and Y. Xiao, *Angew. Chem., Int. Ed. Engl.*, 2021, **60**, 2–26.
7 L. Li, S. Xu, H. Yan, X. Li, H. S. Yazd, X. Li, T. Huang, C. Cui, J. Jiang and W. Tan, *Angew. Chem., Int. Ed. Engl.*, 2021, **60**, 2221–2231.
8 P. J. McCown, K. A. Corbino, S. Stav, M. E. Sherlock and R. R. Breaker, *RNA*, 2017, **23**, 995–1011.
9 E. Braselmann, A. J. Wierzba, J. T. Polaski, M. Chromiński, Z. E. Holmes, S. T. Hung, D. Batan, J. R. Wheeler, R. Parker, R. Jimenez, D. Gryko, R. T. Batey and A. E. Palmer, *Nat. Chem. Biol.*, 2018, **14**, 964–971.
10 J. T. Sczepanski and G. F. Joyce, *Nature*, 2014, **515**, 440–442.
11 T. Walton, S. DasGupta, D. Duzdevich, S. S. Oh and J. W. Szostak, *Proc. Natl. Acad. Sci. U. S. A.*, 2020, **117**, 5741–5748.
12 A. Korman, H. Sun, B. Hua, H. Yang, J. N. Capilato, R. Paul, S. Panja, T. Ha, M. M. Greenberg and S. A. Woodson, *Proc. Natl. Acad. Sci. U. S. A.*, 2020, 117.
13 S. S. S. Panchapakesan and R. R. Breaker, *Nat. Chem. Biol.*, 2021, **17**, 375–382.
14 H. Peng, X. F. Li, H. Zhang and X. C. Le, *Nat. Commun.*, 2017, **8**, 14378.
15 H. Peng, A. M. Newbigging, Z. Wang, J. Tao, W. Deng, X. C. Le and H. Zhang, *Anal. Chem.*, 2018, **90**, 190–207.
16 Z. Yang, K. Y. Loh, Y. T. Chu, R. Feng, N. S. R. Satyavolu, M. Xiong, S. M. Nakamata Huynh, K. Hwang, L. Li, H. Xing, X. Zhang, Y. R. Chemla, M. Gruebele and Y. Lu, *J. Am. Chem. Soc.*, 2018, **140**, 17656–17665.
17 Y. Lin, Z. Yang, R. J. Lake, C. Zheng and Y. Lu, *Angew. Chem., Int. Ed. Engl.*, 2019, **58**, 17061–17067.
18 K. Hwang, Q. Mou, R. J. Lake, M. Xiong, B. Holland and Y. Lu, *Inorg. Chem.*, 2019, **58**, 13696–13708.
19 C. E. McGhee, K. Y. Loh and Y. Lu, *Curr. Opin. Biotechnol.*, 2017, **45**, 191–201.
20 R. J. Lake, Z. Yang, J. Zhang and Y. Lu, *Acc. Chem. Res.*, 2019, **52**, 3275–3286.
21 Y. Xiang and Y. Lu, *Nat. Chem.*, 2011, **3**, 697–703.
22 H. Li, P. Dauphin-Ducharme, G. Ortega and K. W. Plaxco, *J. Am. Chem. Soc.*, 2017, **139**, 11207–11213.
23 J. Zhang, H. Xing and Y. Lu, *Chem. Sci.*, 2018, **9**, 3906–3910.
24 Y. Xiong, J. Zhang, Z. Yang, Q. Mou, Y. Ma, Y. Xiong and Y. Lu, *J. Am. Chem. Soc.*, 2020, **142**, 207–213.
25 L. Zhang, S. Guo, J. Zhu, Z. Zhou, T. Li, J. Li, S. Dong and E. Wang, *Anal. Chem.*, 2015, **87**, 11295–11300.
26 H. Li, P. Dauphin-Ducharme, N. Arroyo-Currás, C. H. Tran, P. A. Vieira, S. Li, C. Shin, J. Somerson, T. E. Kippin and K. W. Plaxco, *Angew. Chem., Int. Ed. Engl.*, 2017, **56**, 7492–7495.

© 2021 The Author(s). Published by the Royal Society of Chemistry

Open Access Article. Published on 09 August 2021. Downloaded on 2/11/2026 8:37:09 PM. This article is licensed under a Creative Commons Attribution-NonCommercial 3.0 Unported Licence.

27 J. Zhang and Y. Lu, *Angew. Chem., Int. Ed. Engl.*, 2018, **57**, 9702–9706.
28 J. Zhang, T. Lan and Y. Lu, *TrAC, Trends Anal. Chem.*, 2020, **124**, 115782.
29 M. Rothenbroker, E. M. McConnell, J. Gu, M. L. Urbanus, S. E. Samani, A. W. Ensminger, C. D. M. Filipe and Y. Li, *Angew. Chem., Int. Ed. Engl.*, 2021, **60**, 4782–4788.
30 J. Canoura, Z. Wang, H. Yu, O. Alkhamis, F. Fu and Y. Xiao, *J. Am. Chem. Soc.*, 2018, **140**, 9961–9971.
31 M. J. Langton, C. J. Serpell and P. D. Beer, *Angew. Chem., Int. Ed. Engl.*, 2016, **55**, 1974–1987.
32 S. Saha, V. Prakash, S. Halder, K. Chakraborty and Y. Krishnan, *Nat. Nanotechnol.*, 2015, **10**, 645–651.
33 M. Cametti and K. Rissanen, *Chem. Soc. Rev.*, 2013, **42**, 2016–2038.
34 Y. Zhou, J. F. Zhang and J. Yoon, *Chem. Rev.*, 2014, **114**, 5511–5571.
35 P. P. Chen, W. Bai and Y. Y. Bao, *J. Mater. Chem. C*, 2019, **7**, 11731–11746.
36 E. A. Martínez-Mier, *J. Evidence-Based Complementary Altern. Med.*, 2011, **17**, 28–32.
37 D. Briancon, *Rev. Rhum. Engl. Ed.*, 1997, **64**, 78–81.
38 O. Barbier, L. Arreola-Mendoza and L. M. Del Razo, *Chem.-Biol. Interact.*, 2010, **188**, 319–333.
39 M. H. Akuno, G. Nocella, E. P. Milia and L. Gutierrez, *J. Water Health*, 2019, **17**, 845–862.
40 B. K. Datta, C. Kar and G. Das, *J. Chem. Sci.*, 2015, **127**, 337–342.
41 B. Spittle, *Fluoride*, 2019, **52**, 7–8.
42 R. Hu, J. Feng, D. Hu, S. Wang, S. Li, Y. Li and G. Yang, *Angew. Chem., Int. Ed. Engl.*, 2010, **49**, 4915–4918.
43 A. Dhillon, M. Nair and D. Kumar, *Anal. Methods*, 2016, **8**, 5338–5352.
44 H. Yahyavi, M. Kaykhaii and M. Mirmoghaddam, *Crit. Rev. Anal. Chem.*, 2016, **46**, 106–121.
45 Y. Jiao, B. Zhu, J. Chen and X. Duan, *Theranostics*, 2015, **5**, 173–187.
46 F. M. Ebrahim, T. N. Nguyen, S. Shyshkanov, A. Gladysiak, P. Favre, A. Zacharia, G. Itskos, P. J. Dyson and K. C. Stylianou, *J. Am. Chem. Soc.*, 2019, **141**, 3052–3058.
47 C. H. Chen and F. P. Gabbaï, *Angew. Chem., Int. Ed. Engl.*, 2018, **57**, 521–525.
48 X. Sun, S. D. Dahlhauser and E. V. Anslyn, *J. Am. Chem. Soc.*, 2017, **139**, 4635–4638.
49 S. Guha and S. Saha, *J. Am. Chem. Soc.*, 2010, **132**, 17674–17677.
50 C. Fang, R. Dharmarajan, M. Megharaj and R. Naidu, *TrAC, Trends Anal. Chem.*, 2017, **86**, 143–154.
51 Y. Guo, J. Li, S. Chai and J. Yao, *Nanoscale*, 2017, **9**, 17667–17680.
52 J. L. Baker, N. Sudarsan, Z. Weinberg, A. Roth, R. B. Stockbridge and R. R. Breaker, *Science*, 2012, **335**, 233–235.
53 A. Ren, K. R. Rajashankar and D. J. Patel, *Nature*, 2012, **486**, 85–89.
54 A. Serganov and E. Nudler, *Cell*, 2013, **152**, 17–24.
55 B. Zhao, S. L. Guffy, B. Williams and Q. Zhang, *Nat. Chem. Biol.*, 2017, **13**, 968–974.
56 M. Chawla, R. Credendino, A. Poater, R. Oliva and L. Cavallo, *J. Am. Chem. Soc.*, 2015, **137**, 299–306.
57 A. East-Seletsky, M. R. O'Connell, S. C. Knight, D. Burstein, J. H. Cate, R. Tjian and J. A. Doudna, *Nature*, 2016, **538**, 270–273.
58 O. O. Abudayyeh, J. S. Gootenberg, P. Essletzbichler, S. Han, J. Joung, J. J. Belanto, V. Verdine, D. B. T. Cox, M. J. Kellner, A. Regev, E. S. Lander, D. F. Voytas, A. Y. Ting and F. Zhang, *Nature*, 2017, **550**, 280–284.
59 A. Pickar-Oliver and C. A. Gersbach, *Nat. Rev. Mol. Cell Biol.*, 2019, **20**, 490–507.
60 J. E. van Dongen, J. T. W. Berendsen, R. D. M. Steenbergen, R. M. F. Wolthuis, J. C. T. Eijkel and L. I. Segerink, *Biosens. Bioelectron.*, 2020, **166**, 112445.
61 Y. Dai, Y. Wu, G. Liu and J. J. Gooding, *Angew. Chem., Int. Ed. Engl.*, 2020, **59**, 20754–20766.
62 J. P. Broughton, X. Deng, G. Yu, C. L. Fasching, V. Servellita, J. Singh, X. Miao, J. A. Streithorst, A. Granados, A. Sotomayor-Gonzalez, K. Zorn, A. Gopez, E. Hsu, W. Gu, S. Miller, C.-Y. Pan, H. Guevara, D. A. Wadford, J. S. Chen and C. Y. Chiu, *Nat. Biotechnol.*, 2020, **38**, 870–874.
63 J. S. Gootenberg, O. O. Abudayyeh, J. W. Lee, P. Essletzbichler, A. J. Dy, J. Joung, V. Verdine, N. Donghia, N. M. Daringer, C. A. Freije, C. Myhrvold, R. P. Bhattacharyya, J. Livny, A. Regev, E. V. Koonin, D. T. Hung, P. C. Sabeti, J. J. Collins and F. Zhang, *Science*, 2017, **356**, 438–442.
64 J. S. Gootenberg, O. O. Abudayyeh, M. J. Kellner, J. Joung, J. J. Collins and F. Zhang, *Science*, 2018, **360**, 439–444.
65 Y. Shan, X. Zhou, R. Huang and D. Xing, *Anal. Chem.*, 2019, **91**, 5278–5285.
66 R. Bruch, J. Baaske, C. Chatelle, M. Meirich, S. Madlener, W. Weber, C. Dincer and G. A. Urban, *Adv. Mater.*, 2019, **31**, e1905311.
67 T. Zhou, R. Huang, M. Huang, J. Shen, Y. Shan and D. Xing, *Adv. Sci.*, 2020, **7**, 1903661.
68 C. M. Ackerman, C. Myhrvold, S. G. Thakku, C. A. Freije, H. C. Metsky, D. K. Yang, S. H. Ye, C. K. Boehm, T. F. Kosoko-Thoroddsen, J. Kehe, T. G. Nguyen, A. Carter, A. Kulesa, J. R. Barnes, V. G. Dugan, D. T. Hung, P. C. Blainey and P. C. Sabeti, *Nature*, 2020, **582**, 277–282.
69 T. Tian, B. Shu, Y. Jiang, M. Ye, L. Liu, Z. Guo, Z. Han, Z. Wang and X. Zhou, *ACS Nano*, 2021, **15**, 1167–1178.
70 Y. Chen, S. Yang, S. Peng, W. Li, F. Wu, Q. Yao, F. Wang, X. Weng and X. Zhou, *Chem. Sci.*, 2019, **10**, 2975–2979.
71 P. Qin, M. Park, K. J. Alfson, M. Tamhankar, R. Carrion, J. L. Patterson, A. Griffiths, Q. He, A. Yildiz, R. Mathies and K. Du, *ACS Sens.*, 2019, **4**, 1048–1054.
72 J. Arizti-Sanz, C. A. Freije, A. C. Stanton, B. A. Petros, C. K. Boehm, S. Siddiqui, B. M. Shaw, G. Adams, T. F. Kosoko-Thoroddsen, M. E. Kemball, J. N. Uwanibe, F. V. Ajogbasile, P. E. Eromon, R. Gross, L. Wronka, K. Caviness, L. E. Hensley, N. H. Bergman, B. L. MacInnis, C. T. Happi, J. E. Lemieux, P. C. Sabeti and C. Myhrvold, *Nat. Commun.*, 2020, **11**, 5921.

© 2021 The Author(s). Published by the Royal Society of Chemistry

Open Access Article. Published on 09 August 2021. Downloaded on 2/11/2026 8:37:09 PM.
This article is licensed under a Creative Commons Attribution-NonCommercial 3.0 Unported Licence.

73 P. Fozouni, S. Son, M. Diaz de Leon Derby, G. J. Knott, C. N. Gray, M. V. D'Ambrosio, C. Zhao, N. A. Switz, G. R. Kumar, S. I. Stephens, D. Boehm, C. L. Tsou, J. Shu, A. Bhuiya, M. Armstrong, A. R. Harris, P. Y. Chen, J. M. Osterloh, A. Meyer-Franke, B. Joehnk, K. Walcott, A. Sil, C. Langelier, K. S. Pollard, E. D. Crawford, A. S. Puschnik, M. Phelps, A. Kistler, J. L. DeRisi, J. A. Doudna, D. A. Fletcher and M. Ott, *Cell*, 2021, **184**, 323–333.

74 C. Myhrvold, C. A. Freije, J. S. Gootenberg, O. O. Abudayyeh, H. C. Metsky, A. F. Durbin, M. J. Kellner, A. L. Tan, L. M. Paul, L. A. Parham, K. F. Garcia, K. G. Barnes, B. Chak, A. Mondini, M. L. Nogueira, S. Isern, S. F. Michael, I. Lorenzana, N. L. Yozwiak, B. L. MacInnis, I. Bosch, L. Gehrke, F. Zhang and P. C. Sabeti, *Science*, 2018, **360**, 444–448.

75 J. Shen, X. Zhou, Y. Shan, H. Yue, R. Huang, J. Hu and D. Xing, *Nat. Commun.*, 2020, **11**, 267.

76 J. Zhou, L. Yin, Y. Dong, L. Peng, G. Liu, S. Man and L. Ma, *Anal. Chim. Acta*, 2020, **1127**, 225–233.

77 R. S. Iwasaki and R. T. Batey, *Nucleic Acids Res.*, 2020, **48**, e101.

78 SW-846 Test Method 9214: Potentiometric Determination of Fluoride in Aqueous Samples with Ion-Selective Electrode, https://www.epa.gov/hw-sw846/sw-846-test-method-9214-potentiometric-determination-fluoride-aqueous-samples-ion-selective, 1996.

79 M. Bader, *J. Chem. Educ.*, 1980, **57**, 703–706.